Hyperfine Interact (2016) 237:70
DOI 10.1007/s10751-016-1216-6

Site analysis and calculation of the quadrupole splitting of Prussian Blue Mössbauer spectra

T. L. Greaves[1,2] · J. D. Cashion[1]

Abstract The insoluble Prussian Blue (IPB) structure, $Fe^{3+}_4[Fe^{II}(CN)_6]_3.14H_2O$, is shown to have ten distinctly different ferric sites, as well as the single ferrous site. The statistical probability of these sites was determined and the point charge model used to calculate the relative quadrupole splitting values. Previous Mössbauer spectra of IPB have fitted the ferric site with one doublet. Our results show that there is a large difference between the quadrupole splittings of the different ferric sites and hence it is not a reasonable approximation to fit them using a single doublet.

Keywords Prussian blue · Crystallography · Mössbauer effect · Point charge calculation · Quadrupole splitting · Electric field gradient

1 Introduction

Prussian Blue is a mixed valence iron cyanide complex, which contains high spin ferric iron and low spin ferrocyanide. The name Prussian Blue (PB) is commonly used to refer to two distinct chemical structures, insoluble Prussian Blue (IPB), $Fe^{3+}_4[Fe^{II}(CN)_6]_3.14H_2O$, and soluble Prussian Blue (SPB), nominally $KFe^{3+}[Fe^{II}(CN)_6]$. The structures are similar, consisting of a cubic arrangement with octahedrally coordinated ferric and ferrocyanide iron. The key difference between them is that the ferric to ferrocyanide iron ratio is 1:1

This article is part of the Topical Collection on *Proceedings of the International Conference on the Applications of the Mössbauer Effect (ICAME 2015), Hamburg, Germany, 13–18 September 2015*

✉ J. D. Cashion
john.cashion@monash.edu

[1] School of Physics and Astronomy, Monash University, Melbourne, Vic 3800, Australia

[2] Present address: School of Applied Sciences, College of Science, Engineering and Health, RMIT University, GPO Box 2476, Melbourne, Victoria 3001, Australia

Published online: 01 March 2016

for SPB and 1.33:1 for IPB. The majority of the Prussian Blue preparation methods lead to colloidal blue particles, which are difficult to characterise.

In the Ludi model [1–6] of the IPB structure, all the ferric sites are occupied and one quarter of the ferrocyanide sites are vacant. This is the general accepted structure for IPB [7–9]. This structure was developed from X-Ray and neutron scattering data taken of crystalline PB and its analogues. In comparison the SPB structure consists of fully occupied ferric and ferrocyanide sites. Ludi has strongly suggested that PB complexes with the SPB formula are actually IPB which has been contaminated with potassium and so PB samples should be considered to have a composition between that of IPB and SPB, depending on the level of potassium present.

Mössbauer spectroscopy has been utilised extensively in the study of PB and its analogues [8–27], with the PB samples usually divided into the two distinct categories of IPB or SPB. However, the fitting of the Mössbauer spectra conventionally utilises a singlet for the perfectly octahedral low spin ferrocyanide site and a doublet for the ferric site. Each valent site has metal neighbours of only the opposite valency. However, in the Ludi Model [1–6] of the IPB structure, all the ferric sites are occupied and one-quarter of the ferrocyanide sites are vacant. These vacant sites are filled by six water molecules and, in addition, there are eight interstitial water molecules. There are thus a considerable number of ferric sites, each of which will have a different electric field gradient (EFG).

The Mössbauer parameters for IPB have generally been poorly reported and none have used multiple doublets for the ferric site. The report by Reguera et al. [26] is the only one which reports both the spectral areas and linewidths. The linewidth of the ferric doublet ranges from 0.606 to 1.00 mm/s in different reports, and the ferrocyanide linewidth ranges between 0.36 to 0.596 mm/s. Typical linewidths for a clean iron site should be less than 0.3 mm/s, so these results are consistent with the premise that there are a number of different ferric sites present, which are in turn affecting the ferrocyanide sites, causing the range of parameters.

This complication means that the conventional fitting of the ferric subspectrum by one doublet is an unjustified simplification. However, there is insufficient resolution to attempt to fit the spectra meaningfully to multiple doublets without additional information. In order to provide this information, we have carried out point charge calculations of the EFG for all the possible ferric coordinations. In a subsequent paper, we will describe their use in the fitting of the Mössbauer spectra of six PB samples and the effect of chemical preference.

2 Crystallographic model

2.1 Iron sites present in IPB

The ferric and ferrous iron ions present in Prussian Blue are all octahedrally coordinated, and are connected by linear Fe^{II}-CN-Fe^{3+} linkages. The iron sites can be represented by Fig. 1, with each iron atom surrounded by six iron sites of the other valency (the cyanide groups have been omitted for clarity).

In the IPB structure all the ferric sites are occupied and one quarter of the ferrocyanide sites are vacant. The six ferrocyanide sites which are vacant are replaced with 14 water molecules, where six waters occupy the cyanide sites, and coordinate to ferric atoms, and the remaining 8 water molecules are uncoordinated. This causes the ferric ion to have the chemical environment $Fe^{3+}(CN)_x(H_2O)_y$, where x+y=6, on average x = 4.5, and y = the

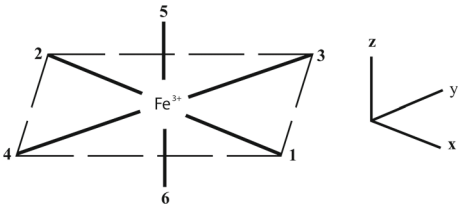

Fig. 1 Fe^{II} sites around a Fe^{3+} atom

number of vacant ferrous sites. In contrast, the ferrocyanide site is always surrounded by six ferric ions.

For the following calculations it was set as a criterion that for any two iron sites to be equivalent, the chemical environment out to these next nearest iron sites had to be identical. The ferrous sites are all surrounded by six ferric ions, and hence are considered equivalent, while the ferric sites are more complicated since the surrounding ferrous sites can be vacant or occupied.

There are ten possible ferric sites which have uniquely different coordinations of water and cyanide ligands. Table 1 describes each of these sites, in terms of whether the six surrounding ferrous iron sites are occupied, O, or vacant, V. The labelling of the ferrous sites is consistent with those in Fig. 1.

The statistical probability in Table 1 for each of the uniquely different iron sites was calculated using the probability of each ligand combination multiplied by the number of ways it can be obtained. It is important to note that these probabilities are only statistical, and do not take into account the chemical properties of the ligands which are expected to modify these numbers by favouring some configurations over others.

2.2 Calculated quadrupole splitting values for the ferric sites in IPB

The quadrupole splitting produced in an iron nucleus is dependent on the electric field gradient (EFG) experienced by the iron nucleus due to the charges of the surrounding atoms. Both the lattice and the valence electrons surrounding each iron nucleus contribute to the EFG experienced, as shown in (1), where R and γ_∞ are the Sternheimer anti-shielding factors.

$$V_{ZZ} = (1 - R)V_{ZZ(val)} + (1 - \gamma_\infty)V_{ZZ(latt)} \tag{1}$$

However, for high spin ferric iron, the valency electron configuration is spherically symmetric and has little direct contribution to the EFG, so the surrounding lattice atoms are the dominant cause of any EFG experienced by the nucleus. This simplifies (1) to give (2), since only the lattice term is non-zero.

$$V_{ZZ} = (1 - \gamma_\infty)V_{ZZ(latt)} \tag{2}$$

While the valency electrons do not contribute directly, they are polarised by the EFG from the lattice, and modify the EFG experienced at the atomic site, by the factor 1-γ_∞.

The point charge model was used to calculate the EFG experienced by the ferric nuclei for each of the possible ferric sites in IPB. Each atom, and cyanide group, was treated as if all their charge was located as a point charge on their lattice site. More sophisticated methods are available for calculating the quadrupole splitting, however there is insufficient crystallographic information to use them for PB.

Table 1 Reference labels assigned to each uniquely different ferric iron site

Fe^{3+} sites		Fe^{II} sites						No. ways	Probability
Label	Ligands	1	2	3	4	5	6		
1	$(CN)_6$	O	O	O	O	O	O	1	0.1780
2	$(CN)_5(H_2O)$	V	O	O	O	O	O	6	0.3560
3	$(CN)_4(H_2O)_2$	V	V	O	O	O	O	3	0.0593
4	$(CN)_4(H_2O)_2$	V	O	V	O	O	O	12	0.2373
5	$(CN)_3(H_2O)_3$	V	V	O	O	V	O	12	0.0791
6	$(CN)_3(H_2O)_3$	V	O	V	O	V	O	8	0.0527
7	$(CN)_2(H_2O)_4$	V	V	V	V	O	O	12	0.0264
8	$(CN)_2(H_2O)_4$	V	V	V	O	V	O	3	0.0066
9	$(CN)(H_2O)_5$	V	V	V	V	V	O	6	0.0044
10	$(H_2O)_6$	V	V	V	V	V	V	1	0.0002

The six numbered sites correspond to the six sites in Fig. 1. O denotes the site is occupied, while V denotes that it is vacant

2.3 Lattice coordinates of the atoms present in IPB

The lattice positions for the different atoms within IPB were based on the crystallographic data of Buser et al. [7] and Herren et al. [9]. While the positions of iron atoms were specified, there was some ambiguity surrounding the positions of the cyanides, and the atoms within the water molecules. Consequently some approximations were made to enable the point charge model to be used.

Each cyanide group was treated as single entity with a charge of negative one, and was assigned the average lattice coordinate of the carbon and nitrogen positions. This is consistent with the strong bond between the carbon and nitrogen atoms in a cyanide molecule which causes them to behave more as a single entity, than as individual atoms.

2.4 Location of the water molecules

There are ideally 14 water molecules per unit cell according to the IPB structure, and three possible locations for them. This causes serious complications in determining the exact atomic positions for use in the point charge model. Six of the water molecules per unit cell are located in the vacant cyanide sites, which will be referred to as water-1 sites, and these waters are bonded to ferric iron atoms. The remaining eight water molecules can be in either water-2 or water-3 sites, and the exact location of these waters appears to be sample dependent [9], with more details given in Herren et al. [9].

For the point charge model calculations it was approximated that the eight non-structural water molecules were all located in water-2 sites, with none in water-3 sites. There were two main reasons for this choice. First, the water-2 sites are energetically favourable compared to the water-3 sites, due to a hydrogen bond between the oxygen in the water-2 and a hydrogen atom in the water-1. Secondly, a combination of water-2 and water-3 sites would be

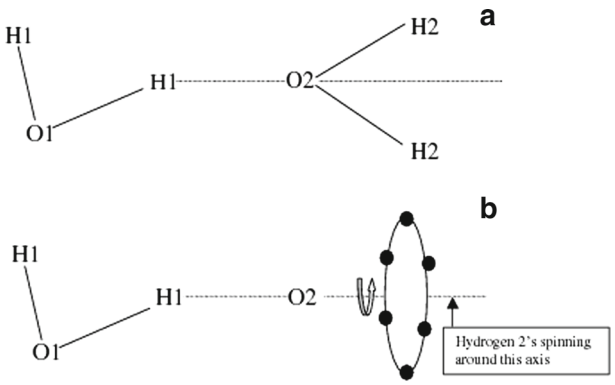

Fig. 2 Determining the hydrogen-2 positions. **a** Locating the H2's at a maximum distance from the H1's, while maintaining the bond angle at 112° [6], and **b** six positions used to approximate the H2's rotating

extremely complex to model, since the exact ratio of water-2 and water-3 molecules would not be constant for each ferrocyanide vacancy.

The positions of the oxygen and hydrogen atoms for the water-1 sites were given by Herren et al. [9]. The position of the oxygen and hydrogen atoms for the water-2 sites needed to be approximated since there was no available information about the exact location, and the following procedure was used:

(1) The bond length O2-H2 and bond angle H2-O2-H2 for water-2 were assumed to be the same as for the water-1 molecules.
(2) The O1 - water-2 bond length was taken to define the distance between O1 and O2, since the O2 atoms were assumed to be located at the position given for the water-2 sites.
(3) The O2's were assumed to be hydrogen-bonded to the nearest hydrogen atom of the water-1 sites.
(4) The H2's were assumed to be as far away from the H1's as possible, since there were no other nearby atoms to influence their positions.

This gives rise to the arrangement in Fig. 2, except that the H2 atoms are not uniquely positioned. They can be anywhere on a circle and arranged 180° apart. It seemed most likely that the hydrogens are actually rotating around this circle, which is consistent with Buser et al. not being able to determine their exact locations [8]. Six positions around the circle, evenly spaced at 60° intervals, were used to represent the averaging of the two H2's, each with an effective charge of +1/3, shown in Fig. 2b.

3 The EFG tensor matrices

The lattice electric field tensor components were calculated using (3) for each of the ferric sites, where Z(n) is the charge on the nth atom, r is the distance of the nth atom from the site of interest and δ_{ij} is the Kronecker δ-function. This resulted in a 3 × 3 matrix for each ferric site.

$$V_{ij(latt)} = \frac{1}{4\pi\varepsilon_0} \sum_{ij} Z(n) \frac{3x_i x_j - \delta_{ij} r^2}{r^5} \; ; \quad x_i x_j = x, y, z \tag{3}$$

Table 2 Eigenvalues and eigenvectors for each of the iron sites, in terms of lattice directions

Iron site	EFG axes	Eigenvalues ($Å^{-3}$)	Eigen vectors			Princ. axes
			X	Y	Z	
2	Z	0.176	1.000	0.000	0.000	[1 0 0]
	Y	0.108	0.000	0.707	0.707	
	X	0.069	0.000	0.707	−0.707	
3	Z	−0.353	1.000	0.000	0.000	[1 0 0]
	Y	0.176	0.000	0.000	1.000	
	X	0.176	0.000	1.000	0.000	
4	Z	0.179	0.059	−0.072	−0.997	[0 0 1]
	Y	−0.091	−0.626	0.774	−0.093	
	X	−0.088	−0.777	−0.629	0.000	
5	Z	0.265	−0.037	−1.000	0.000	[0 1 0]
	Y	−0.268	−1.000	0.037	0.000	
	X	0.000	0.000	0.000	1.000	
6	Z	−0.036	0.565	−0.602	0.565	∼ [1 1 1]
	Y	0.021	−0.426	−0.799	−0.426	
	X	0.016	0.707	0.000	−0.707	
7	Z	0.353	0.000	0.000	1.000	[1 0 0]
	Y	−0.176	1.000	0.000	0.000	
	X	−0.176	0.000	1.000	0.000	
8	Z	−0.179	−1.000	0.072	−0.059	[1 0 0]
	Y	0.091	0.093	0.774	−0.626	
	X	0.088	0.000	0.629	0.777	
9	Z	0.176	0.000	0.000	1.000	[0 0 1]
	Y	−0.108	−0.707	0.707	0.000	
	X	−0.069	0.707	0.707	0.000	

Princ. axes refers to the approximate direction of the principal axis for each iron site

The ferric sites 1 and 10, which are surrounded by six cyanides and six waters respectively, both have cubic symmetry, and hence a zero EFG, and zero quadrupole splitting. All the other ferric sites have a combination of cyanide and water ligands which lead to a non-zero EFG. Only the ferric sites with a non-zero EFG are treated below.

All atoms within a cube of $3 \times 3 \times 3$ unit cells centred on the ferric atom were included in the calculations. For each calculation, the ferric atom of interest was located at the centre of the middle unit cell. All distances, r, to the surrounding atoms were taken relative to this ferric atom. The charge of an atom, Z(n), was modified for atoms on the face, edge or corner of a unit cell, where the fractional charge of 1/2, 1/4 or 1/8, respectively, of the real charge was used. This ensured an electrically neutral block.

The EFG contribution was calculated separately for each atom within the $3 \times 3 \times 3$ unit cells surrounding the ferric iron atom, and the resulting sum led to 3×3 matrices describing the EFG experienced at the ferric atom site due to the surrounding atoms. The 3×3 matrices of the EFG tensor components were diagonalised to obtain the eigenvalues and eigenvectors for each iron site, which are given in Table 2. The iron site numbers refer to each iron site identified in Table 1. The eigenvalues and eigenvectors are given in terms of

Table 3 Theoretical quadrupole splitting values for the ferric sites

Ferric site	$V_{ZZ}(V/m^2)$	η	QS (mm/s)
1	0	0	0
2	-2.53×10^{20}	0.22	0.300
3	-5.08×10^{20}	0.00	0.596
4	2.58×10^{20}	0.01	−0.302
5	-3.82×10^{20}	1.00	0.517
6	-0.52×10^{20}	0.14	0.062
7	5.08×10^{20}	0.00	−0.596
8	-2.58×10^{20}	0.01	0.302
9	2.53×10^{20}	0.22	−0.300
10	0	0	0

the lattice coordinate system. There are many other equivalent sites which can be obtained through a rotation of the lattice. Regardless of these rotations, each of these sites will have eigenvalues of the same magnitude as their equivalent site, and the eigenvector will simply need to undergo the same rotation as the lattice. These equivalent sites will produce the same quadrupole splittings.

In order to conform to the Mössbauer conventions, the three eigenvalues must have their axes relabelled to make $|V_{ZZ}| \geq |V_{XX}| \geq |V_{YY}|$. These axes may, but need not, align with the crystal axes. This relabelling ensures that the asymmetry parameter, η, satisfies $0 \leq \eta \leq 1$. The approximate crystallographic direction of the principal axis of the EFG for each iron site has been included in Table 2.

The lattice Vzz and η values were used to calculate the quadrupole splittings (QS), and the results for the different sites, including the enhancement by the Sternheimer antishielding factor, are given in Table 3. The value of the Sternheimer factor, γ_∞, used for high spin ferric iron was −9.427 [28].

While the quadrupole splittings include both positive and negative numbers, only the magnitudes are of importance when fitting Mössbauer spectra containing only doublets. Sites 2 and 9, as well as 3 and 7, and 4 and 8, differ only in sign. This is because they are matching pairs with a direct swap of the vacant and occupied sites in Table 1.

The quadrupole splitting values obtained cannot be used directly to fit the spectra. While it is expected that the calculation will have produced the correct relative magnitude, it is necessary to scale all the values by comparing them with experimental spectra in order to compensate for having used the point charge model approximation. This will be carried out in a subsequent paper where we use these values to fit appropriate PB Mössbauer spectra.

It is clear from Table 3 that there are a number of discrete and different quadrupole splitting values corresponding to the ferric sites in PB. Hence the traditional method of fitting the ferric sites in the Mössbauer spectra using a single Lorentzian doublet is a poor approximation to the complexity of the structure.

4 Conclusion

The IPB structure has been shown to contain ten distinctly different ferric sites and one ferrocyanide site. The point charge model has been used to calculate the relative quadrupole

splitting values for each of these ferric sites. The large range of the predicted quadrupole splitting values from zero up to a nominal value of 0.6 mm/s shows that more than one doublet is required to fit the Mössbauer spectra of PB. These values will be used as the basis for fitting the experimental Mössbauer spectra of PB samples.

Acknowledgments This research has been supported by the School of Physics, Monash University. TLG acknowledges the receipt of an Australian Postgraduate Award.

References

1. Ludi, A., Gudel, H.-U., Ruegg, M.: Die strukter der hydrate von $Co_3[Co(CN)_6]_2$ und $Cd_3[Co(CN)_6]_2$. Helv. Chim. Acta **51**, 2006 (1968)
2. Ludi, A., Gudel, H.-U., Ruegg, M.: The structural chemistry of Prussian Blue analogs. A single crystal study of manganese(II) hexacyanocobaltate(III) $Mn_3[Co(CN)_6]_2.xH_2O$. Inorg. Chem. **9**, 2224–2227 (1970)
3. Ludi, A., Gudel, H.-U.: Structural chemistry of polynuclear transition metal cyanides. Struct. Bond. **14**, 1–21 (1973)
4. Buser, H.J., Ludi, A., Fischer, P., Studach, T., Dale, B.W.: A neutron diffraction study of Prussian Blue, $Fe_4[Fe(CN)_6]_3.14D_2O$. Z. Physik. Chem. **92**, 354–357 (1974)
5. Buser, H.J., Schwarzenbach, D., Petter, W., Ludi, A.: The crystal structure of Prussian Blue: $Fe_4[Fe(CN)_6]_3.xH_2O$. Inorg. Chem. **16**, 2704–2710 (1977)
6. Herren, F., Fischer, P., Ludi, A., Hälg, W.: Neutron diffraction study of Prussian Blue, $Fe_4[Fe(CN)_6]_3.xH_2O$. Inorg. Chem. **19**, 956–959 (1980)
7. Karyakin, A.A.: Prussian Blue and its analogues: electrochemistry and analytical applications. Electroanalysis **13**, 813–819 (2001)
8. Agrisuelas, J., García-Jareño, J.J., Giminez-Romero, D., Vicente, F.: Insights on the mechanism of insoluble-to-soluble Prussian Blue transformation. J. Electrochem. Soc. **156**, P149–P156 (2009)
9. Rykov, A.I., Wang, J., Zhang, T., Nomura, K.: Cs sorption by "soluble" and "insoluble" iron hexacyanocobaltates probed by Mössbauer spectroscopy. Hyperfine Interact. **218**, 53–58 (2013)
10. Epstein, L.M.: Mössbauer spectra of some iron complexes. J. Chem. Phys. **36**, 2731–2737 (1962)
11. Champion, A.R., Drickamer, H.G.: Effect of pressure on the Mössbauer resonance in potassium ferrocyanide, potassium ferricyanide and insoluble Prussian Blue. J. Chem. Phys. **47**, 2591–254 (1967)
12. Ito, A., Suenaga, M., Ono, K.: Mössbauer study of soluble Prussian Blue, insoluble Prussian Blue and Turnbull's blue. J. Chem. Phys. **48**, 3597–3599 (1968)
13. Maer, K. Jr., Beasley, M.L., Collins, R.L., Milligan, W.O.: The structure of the titanium-iron cyanide complexes. J. Am. Chem. Soc. **90**, 3201–3208 (1968)
14. Fung, S.C., Drickamer, H.G.: Effect of pressure on the C-Fe bond in ferrocyanides and ferricyanides. J. Chem. Phys. **51**, 4353–4435 (1969)
15. Fenger, J., Maddock, A.G., Siekierska, K.E.: Chemical consequences of the nuclear reactions $^{58}Fe(n,\gamma)^{59}Fe$ and $^{57}Co(EC)^{57}Fe$ in soluble Prussian Blue. J. Chem. Soc. (A), 3255–3261 (1970)
16. Bonnette, A.K. Jr., Allen, J.F.: Isotopic labelling for Mössbauer studies. An application to the iron cyanides. Inorg. Chem. **10**, 1613–1616 (1971)
17. Allen, J.F., Edwards, B.R., Bonnette, A.K. Jr.: A comparison of two Prussian Blue models. Tracer and Fe-56 labeled Mössbauer studies. J. Inorg. Nucl. Chem. **35**, 3547–3556 (1973)
18. Allen, J.F., Bonnette, A.K. Jr.: Thermal decomposition of Prussian Blue: isotopic labelling with Mössbauer-inactive Fe-56. J. Inorg. Nucl. Chem. **36**, 1011–1016 (1974)
19. Inoue, H., Flück, E., Shirai, T., Yanagisawa, S.: Mössbauer emission spectroscopic characterization of Prussian Blue analogues. J. Phys. **40**(C2), 361–362 (1979)
20. Goldanskii, V.I., Stukan, R.A.: Mössbauer emission spectroscopy studies of tunneling chemical relaxation. J. Phys. **41**(C1), 43–50 (1980)
21. Itaya, K., Akahoshi, H., Toshima, S.: Electrochemistry of Prussian Blue modified electrodes: an electrochemical preparation method. J. Electrochem. Soc.: Electrochem. Sci. Technol. **129**, 1498–1500 (1982)
22. Rasmussen, P.G., Meyers, E.A.: An investigation of Prussian Blue analogues by Mössbauer spectroscopy and magnetic susceptibility. Polyhedron **3**, 183–190 (1984)

23. Wei, H.H., Pan, W.B.: Mössbauer studies of photochemical products of $Ru(bpy)_3^{2+}$ iron cyanide double complexes. Hyperfine Interact. **40**, 359–362 (1988)
24. Inoue, H., Nakazawa, T., Mitsuhashi, T., Shirai, T., Flück, E.: Characterization of Prussian Blue and its decomposition products. Hyperfine Interact. **46**, 725–731 (1989)
25. Nakazawa, T., Inoue, H., Shirai, T.: Comparison of characteristic temperatures determined by Mössbauer spectroscopy and X-ray diffraction. Hyperfine Interact. **55**, 1145–1150 (1990)
26. Reguera, E., Fernáandez-Bertrán, J., Dago, A., Díaz, C.: Mössbauer spectroscopy study of Prussian Blue from different provenances. Hyperfine Interact. **73**, 295–308 (1992)
27. Varret, F., Goujon, A., Bleuzen, A.: Magnetic metastability of the photo-induced state of $C_x^I Co[Fe(CN)_6]_y$ Prussian Blue analogues. Hyperfine Interact. **134**, 69–80 (2001)
28. Su, Z., Coppens, P.: Evaluation of Sternheimer nuclear quadrupole shielding functions and their application to the determination of the $^{57}Fe^m$ nuclear quadrupole moment from X-ray-determined charge densities. Acta Cryst. **A52**, 748–756 (1996)